Bioorganic & Medicinal Chemistry 17 (2009) 6728–6737

Contents lists available at ScienceDirect

Bioorganic & Medicinal Chemistry

journal homepage: www.elsevier.com/locate/bmc

Substituted 2-arylbenzothiazoles as kinase inhibitors: Hit-to-lead optimization

Stefan Tasler [a], Oliver Müller [a], Tanja Wieber [a], Thomas Herz [a], Stefano Pegoraro [a], Wael Saeb [a], Martin Lang [a], Rolf Krauss [a,*], Frank Totzke [b], Ute Zirrgiebel [b,†], Jan E. Ehlert [b], Michael H. G. Kubbutat [b], Christoph Schächtele [b]

[a] 4SC AG, Am Klopferspitz 19a, 82152 Planegg-Martinsried, Germany
[b] ProQinase GmbH, Breisacher Str. 117, 79106 Freiburg, Germany

ARTICLE INFO

Article history:
Received 13 May 2009
Revised 17 July 2009
Accepted 22 July 2009
Available online 25 July 2009

Keywords:
Cancer
Protein kinase
vHTS
Multi-target approach

ABSTRACT

Based on an (aminoaryl)benzothiazole quinazoline hit structure for kinase inhibition, a systematic optimization program resulted in a lead structure allowing for inhibitory activities in cellular phosphorylation assays in the low nanomolar range.

1. Introduction

Within our kinase inhibitor program, a quinazoline-bound 4-(benzothiazol-2′-yl)aniline hit structure had been identified, giving rise to most promising inhibitory activities in in vitro kinase assays on Aurora kinases and EGFR (Table 1).[1] Serine/Threonine and tyrosine kinases of the Aurora and ErbB family, respectively, are described to be potential targets for treating different kind of cancer diseases like colorectal or non-small-cell lung cancer, glioblastoma, breast and colon cancer.[2–6] Aurora A and B expression is low or undetectable in resting cells, they play crucial roles in the G2 and mitotic phases of the cell cycle, and were found to be overexpressed in certain cancer types.[7] Their inhibition results in cell-cycle arrest or apoptosis.[2,7] EGFR (=ErbB1, HER1) and ErbB2 (=HER2) possess multiple modes of action and are involved in signal transduction cascades affecting, for example, cell proliferation, survival, angiogenesis and metastasis.[4–6] These kinases are (over)-expressed in a wide range of solid tumours, thus their inhibition occurred to be a valuable approach for treating respective cancer types. First small molecule protein kinase inhibitors have already been approved by the FDA for cancer treatment, among those Imatinib (Bcr-Abl), Gefitinib (Iressa, EGFR; Fig. 1), Erlotinib (Tarceva, EGFR; Fig. 1), Lapatinib (EGFR/ErbB2) and Sorafenib (multi-target).[6,8]

For an enhancement of efficacy on cancer cells it seemed to be reasonable not to screen for compounds displaying high selectivity for one certain kinase, but rather to address a few selected targets important in same or different stages of tumour progression.[9] EGFR for example, might occur in heterodimers with other members of the ErbB family, which can be even more oncogenic than the respective homodimers. Thus, high inhibitory activities on both kinases, EGFR and ErbB2, seemed desirable rather than tuning highly selective EGFR inhibitors.[6,10]

Table 1
In vitro IC_{50} values [μM] on selected kinases for the initial hit series

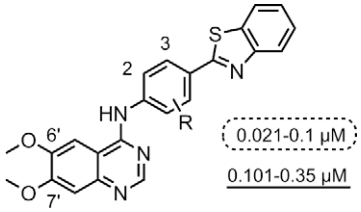

Entry	R	Proliferation			Angiogenesis	
		Aurora A	Aurora B	EGFR	VEGFR2	TIE2
1	H	0.350	0.135	1.500	6.300	n.d
2[a]	2-Me	4.400	3.700	0.240	3.400	0.840
3	3-OH	>10	4.200	2.200	6.900	n.d
4	3-OMe	>10	>10	0.063	>10	n.d

[a] No inhibitory activity on PDGFRβ up to a concn of 100 μM.

* Corresponding author. Tel.: +49 89 700763 0; fax: +49 89 700763 29.
E-mail address: rolf.krauss@4sc.com (R. Krauss).
† Present address: iOMEDICO AG, Hanferstr. 28, 79108 Freiburg, Germany.

0968-0896/$ - see front matter © 2009 Elsevier Ltd. All rights reserved.
doi:10.1016/j.bmc.2009.07.047

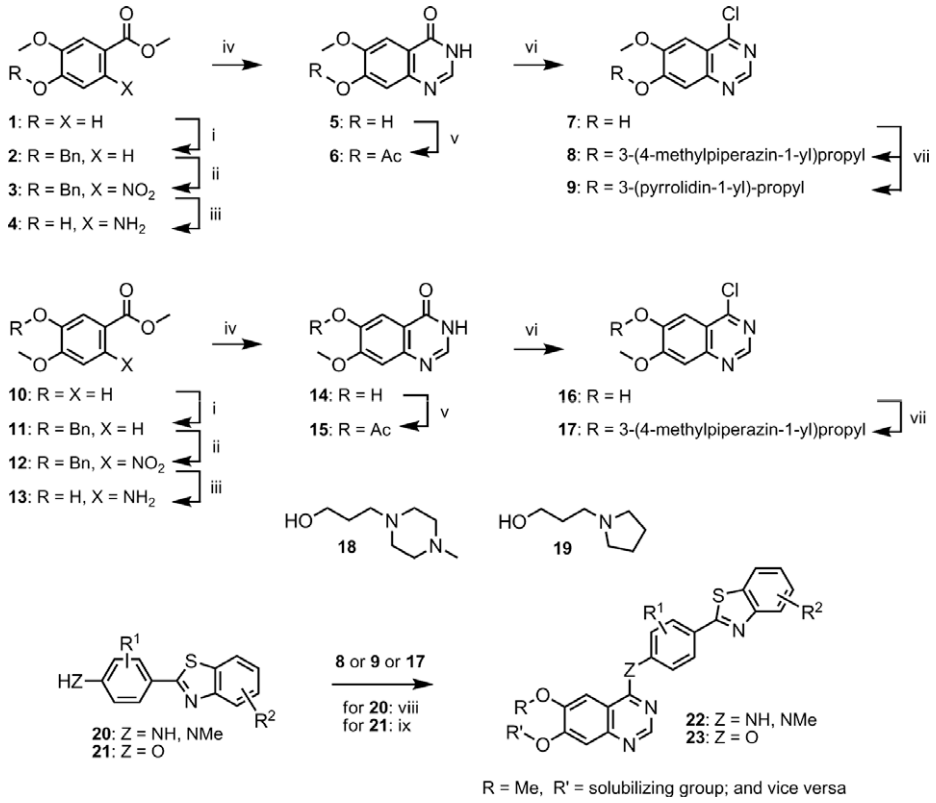

Scheme 1. Synthesis of kinase inhibitors. Reagents and conditions: (i) BnBr, K_2CO_3, DMF, 100 °C, 3 h, quantitatively; (ii) 70% HNO_3, AcOH, 50 °C, 3 h, 91–94%; (iii) H_2 (1 bar), Pd-C, MeOH, rt, ~5 h, quantitatively; (iv) $HCONH_2$, HCO_2NH_4, 140 °C, 4 h, 76–85%; (v) Ac_2O, pyridine, 100 °C, 4 h, 93–96%; (vi) $SOCl_2$, cat. DMF, 85 °C, 1.5 h, then aq NH_3, MeOH, 80 °C, 10 min, up to ~90%; (vii) **18** resp. **19**, PPh_3, DBAD, THF or CH_2Cl_2, rt, 12 h, 65–85%; (viii) HCl, ethylene glycol, 110 °C (in cases of sterical hindrance: up to 140 °C), 3 h, 3–74%; (ix) **21**, NaH, DMSO, 0 °C→rt, then **8** resp. **9**, 130 °C, 12 h, 16–22%.

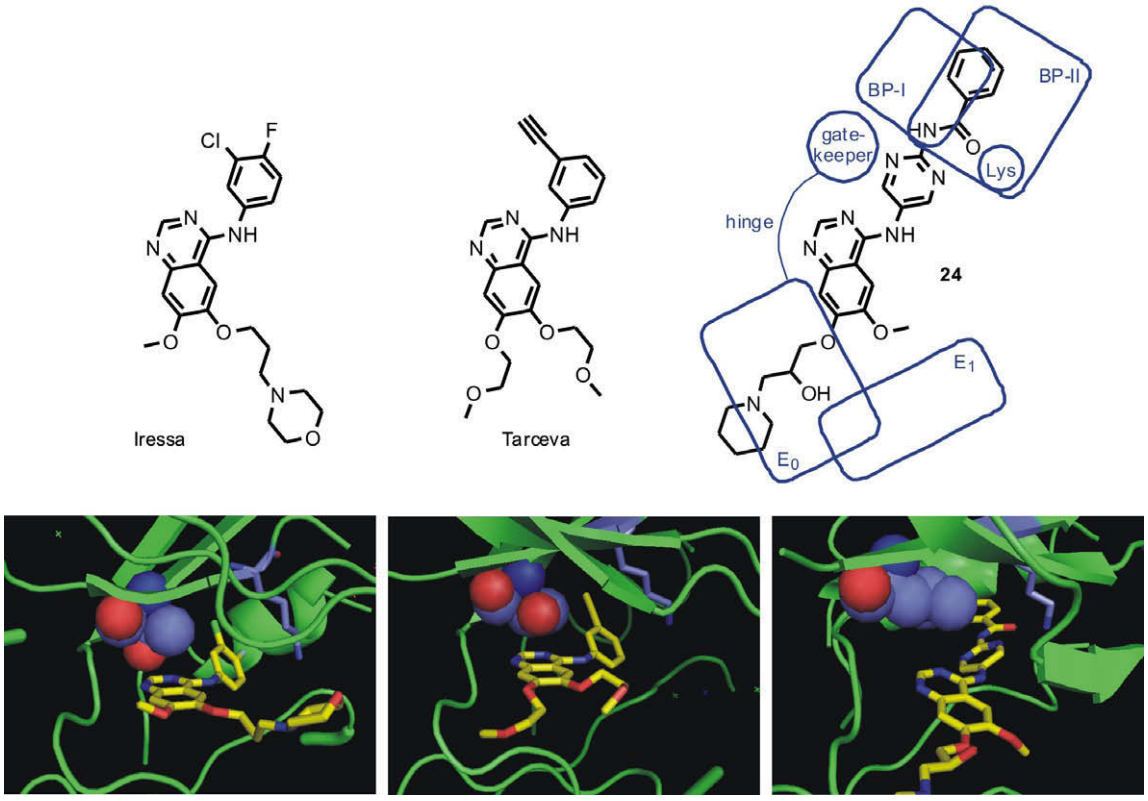

Figure 1. Binding mode of 4-arylamino-quinazolines in EGFR (Iressa, Tarceva) and Aurora A (compound **24**); schematic of binding pockets according to Liao in blue; crystal structures: gatekeeper residue in blue spheres, conserved lysine residue in blue sticks.

Table 2
Selection of kinases for initial screening; size of the gatekeeper residue: 1 = small to 4 = large (for a discussion, see Section 2.3.1)

Function	Kinase	Gatekeeper residue	Size	Kinase subclass
Proliferation	Aurora A	Leu	2	Ser/Thr
	Aurora B	Leu	2	Ser/Thr
	CDK2	Phe	4	Ser/Thr
	CDK4	Phe	4	Ser/Thr
	EGFR	Thr	1	Tyr
	ErbB2	Thr	1	Tyr
	PDGFRβ	Thr	1	Tyr
	PLK1	Leu	2	Ser/Thr
Survival	Akt1	Met	3	Ser/Thr
	IGF1R	Met	3	Tyr
Angiogenesis	VEGFR2	Val	1	Tyr
	VEGFR3	Val	1	Tyr
	TIE2	Ile	2	Tyr
	EphB4	Thr	1	Tyr
Metastasis	FAK	Met	3	Tyr
	c-Src	Thr	1	Tyr
	InsR	Met	3	Tyr

Based on our initial investigations into inhibition profiles for different adenine mimics being N-attached to 4-(benzothiazol-2′-yl)- and 3-(benzothiazol-2′-yl)-anilines, quinazoline scaffolds proved to be promising for further optimization attempts.[1] As an excellent starting point the 6′,7′-dimethoxyquinazoline unit was identified (Table 1), giving rise to in vitro IC_{50} values down to 135 nM on Aurora B (entry 1) and even 63 nM on EGFR (entry 4)—even though with virtually no inhibition of ErbB2. The 4′-(arylamino)-quinazoline structure is already known to possess a potential for good to excellent inhibitory activities on EGFR,[10,11] which was confirmed in our series as well. For initial screening in in vitro kinase activity assays[12] of molecules synthesized, a selection of 16 kinases had been specified, covering different stages of tumour progression (Table 2; plus InsR, inhibition of which had to be avoided as its function is essential for nearly every cell's general response to insulin). In this contribution, we describe further advancement of our multi-target approach to deliver highly potent kinase inhibitors on an enzymatic and also cellular level, displaying intriguing selectivity profiles.

2. Results and discussion

2.1. Synthesis and in vitro inhibition data of new quinazoline derivatives

Original solubility issues of the previously identified hit molecules were first addressed by attachment of solubilizing groups in either the 6′- or the 7′-position of the quinazoline scaffold, which—simultaneously—might tune inhibitory activity and selectivity.[10] These substituents would either point out towards the solvent-exposed entrance E_1 (nomenclature according to Liao, cf. Fig. 1)[8] when attached to 6′-O or would address the secondary hydrophobic patch E_0 offering a certain diversity in sequence and conformation among kinases, when being positioned in the 7′-position of the quinazoline.[8] The success of such an approach is illustrated by, for example, Iressa (Fig. 1), a potent EGFR/ErbB2 inhibitor.[4,13] Synthesis of appropriately substituted 4-chloroquinazolines **8**, **9** and **17** was achieved by a combination of established literature procedures starting from either methyl vanillate (**1**) or methyl isovanillate (**10**), with the only difference towards these protocols being an earlier removal of a benzyl protective group simultaneously with the reduction of the nitro group (Scheme 1).[14–16] Accordingly, quinazolinones **5** and **14** were formed by Niementowski reaction[17] of anthranilates **4** resp. **13** with formamide. Subsequent treatment with $SOCl_2$ required transitory O-acetylation to proceed smoothly. Propanols **18** and **19**, attained by reaction of 3-chloropropanol with *N*-methylpiperazine and pyrrolidine, respectively,[18] were attached to **7** and **16** by Mitsunobu reaction.[16] Chloroquinazolines **8**, **9** and **17** were converted into the final products **22** by heating in ethylene glycol in the presence of the corresponding 4-(benzothiazol-2′-yl)-anilines **20** (Z = NH), succeeding only upon addition of 2.0 equiv of HCl[19] (4.0 M in dioxane), which had to be added to quench both basic nitrogens of the piperazine unit in order to allow for an acceleration of the reaction rate by chloroquinazoline activation by HCl formed during the reaction. Diarylethers **23** were obtained by reaction of 4-(benzothiazol-2′-yl)phenols **21** with suitable chloroquinazolines in the presence of NaH.[20] Required 2′-(4-aminoaryl)benzothiazoles **20** and 4-(benzothiazol-2′-yl)phenols **21** were prepared by polyphosphoric acid mediated condensation of appropriately substituted 2-aminothiophenols with 4-aminobenzoic resp. 4-hydroxybenzoic acid derivatives.[21]

Attaching a solubility enhancer to the 7′-position generally resulted in a significant increase in inhibitory activity (Table 3). Simultaneously, selectivity was lost as compared to the 6′,7′-dimethoxyquinazoline derivatives (Table 1). Inhibition of EGFR and ErbB2 were now very similar, which is in contrast to the corresponding data attained for the 6′,7′-dimethoxyquinazolines of Table 1 and—not as emphasized, though—for those derivatives with the solubility enhancer attached to the 6′-position (Table S1, Supplementary data). With highly conserved binding pockets I and II (BP-I and BP-II, respectively; cf. Fig. 1),[22] such a finding has to be a result of slightly different orientations of molecules with a solubilizing group being attached to the 7′-position as compared to those with 7′-OMe based on the additional binding into pocket E_0 in somewhat different overall conformations of the EGFR and ErbB2 pockets.

When inhibition by compounds of entries 1–4 (Table 1) are compared to those of the respective derivatives in Table 3 (entries 5, 6, 12 and 13, respectively), a decrease of the IC_{50} values by a factor above 20 was observed for the most pronounced targets. Furthermore, best inhibitions were not necessarily detected for identical kinases within such a pair of compounds: a shift from Aurora B to VEGFR2 and Aurora A (entry 1 vs 5), from EGFR to TIE2 (entry 2 vs 6) or from no clearly highlighted preferential kinase to Aurora A and B (entry 3 vs 12) was observed.

In general, inhibition was now found to occur with IC_{50} values below 100 nM for most pronounced targets, in a few cases even down to the one-digit nanomolar range (entry 13, on EGFR and ErbB2; entry 14, on Aurora A and TIE2). A certain preference was identified on kinases crucial for cell proliferation (Aurora A and B, EGFR and ErbB2), and some scattered inhibition of kinases involved in angiogenesis was determined, especially of TIE2. Within the arylbenzothiazole scaffold, further substitution in 3-position of the aryl unit resulted in inhibitory profiles rather similar to the unsubstituted derivative (entries 11–15 vs 5), with a strong emphasis on Aurora A and B, EGFR, ErbB2 and TIE2, whereas 2-substitution gave mainly less active but more selective compounds, especially with a significantly decreased inhibition of EGFR and ErbB2 (entries 6–8 and 10 vs 11–14). Just by varying this substitution pattern using the same substituent (R = OMe), an interesting switch from a rather selective Aurora A and B inhibitor with IC_{50} values of 65 and 90 nM, respectively (entry 8, 2-OMe), to a highly potent and selective EGFR/ErbB2 inhibitor (entry 13, 3-OMe; IC_{50} values of 2 and 5 nM, respectively) was observed. Such a notion might be explained by different dihedral angles adopted around the anilinic NH by the quinazoline versus the aryl plain in combination with the nature of the gatekeeper residues present in the

Table 3
In vitro IC_{50} values (μM) on selected kinases out of a panel of 16

	Entry	R	Proliferation					Angiogenesis			Metastasis
			Aurora A	Aurora B	EGFR	ErbB2	PDGFRβ	VEGFR2	VEGFR3	TIE2	
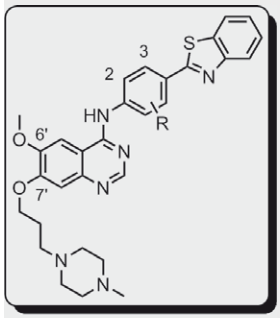	5	H	0.014	0.060	0.046	0.100	1.400	0.012	0.069	0.054	>10
	6	2-Me	0.340	0.440	0.250	0.490	6.700	0.250	0.340	0.038	0.380
	7	2-OH	0.230	0.270	0.350	3.600	>10	0.280	4.500	0.230	8.600
	8	2-OMe	0.065	0.090	>10	>10	5.100	3.300	1.700	0.330	0.740
	9	2-OCF_3	0.290	0.520	>10	>10	9.100	>10	>10	0.590	>10
	10	2-F	0.026	0.028	0.805	2.400	4.400	0.062	0.350	0.029	1.900
	11	3-Me	0.230	0.260	0.032	0.032	7.900	0.350	1.500	0.068	3.400
	12	3-OH	0.091	0.059	0.110	0.780	4.500	0.380	0.520	0.120	>10
	13	3-OMe	0.120	0.300	0.002	0.005	2.100	1.200	7.100	0.110	0.230
	14	3-F	0.009	0.027	0.430	0.300	2.100	0.044	0.210	0.009	>10
	15	3-Cl	0.027	0.078	0.016	0.038	3.600	0.120	0.470	0.037	>10

≤ 0.02 μM
0.021-0.1 μM

Aurora and ErbB kinases (vide infra) and potential hydrogen bonding towards the latter residue.

Attachment of R = 2-OH (entry 7) resulted in a general loss of inhibitory effects, most detrimental proved to be the incorporation of a 2-trifluoromethoxy group (entry 9). Substitution with R = Me or F in either position (entries 6, 10, 11 and 14) generated compounds with the ability to inhibit TIE2 with excellent IC_{50} values between 9 and 68 nM. None or only further substitution with small groups like fluoro in either 2- or 3-position was tolerated within VEGFR2 inhibitors to give IC_{50} values below 100 nM (entries 5, 10 and 14).

With a solubility enhancer being present in the 6′-position, clearly unfavourable inhibitory activities were achieved compared to the derivatives with such a group being placed in the 7′-position (Table S1, Supplementary data vs Table 3). Obviously the loss of binding energy within the hydrophobic patch E_0 by shifting the piperazine unit into the 6′-position cannot be compensated adequately. General SAR trends seemed to be comparable within these two series, though.

Substitution in the distal ring of the benzothiazole unit displayed a clear selectivity enhancing effect for Aurora A and B, since inhibition of other kinases like EGFR/ErbB2 and VEGF receptors decreased significantly (Table 4). Only the R^4 = 6″-OMe or 6″-F derivatives were exceptions with IC_{50} values on EGFR, ErbB2 and TIE2 or VEGFR2 and TIE2, respectively, still being below 400 nM (entries 16 and 17). With the solubility enhancing group being attached to the 7′-position of the quinazoline, inhibition of Aurora kinases remained comparable to the benzothiazole-unsubstituted compound (Table 3, entry 5). Representatives of the 6′-attachment series displayed again decreased inhibitions (Table S1, Supplementary data). A combination of substituents in both aromatic rings of the arylbenzothiazole moiety has just been initiated, a first data point is represented by entry 21: Inhibition of Aurora kinases was slightly decreased by a factor of 3 compared to R^1 = 2-F, R^2 = H

Table 4
In vitro IC_{50} values (μM) on selected kinases out of a panel of 16

	Entry	R^1	R^2	Proliferation					Angiogenesis		
				Aurora A	Aurora B	EGFR	ErbB2	PDGFRβ	VEGFR2	VEGFR3	TIE2
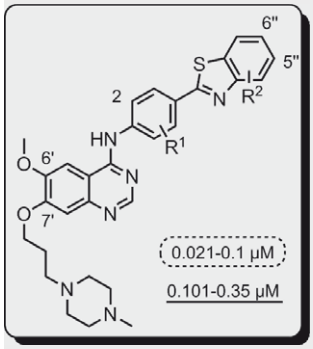	16	H	6”-OMe	0.062	0.048	0.200	0.130	>10	0.690	1.900	0.390
	17	H	6”-F	0.026	0.041	0.730	6.950	3.400	0.335	0.865	0.235
	18	H	6”-Cl	0.054	0.064	0.260	2.300	8.000	2.500	9.300	0.410
	19	H	5”-Cl	0.024	0.062	>10	>10	>10	0.610	1.300	0.510
	20	H	5”-CF_3	0.060	0.120	>10	>10	8.200	>10	>10	3.300
	21	2-F	6”-Cl	0.085	0.090	6.200	>10	9.200	2.250	3.000	0.615

0.021-0.1 μM
0.101-0.35 μM

(Table 3, entry 10) or by a factor of 1.5 over R^1 = H, R^2 = 6″-Cl (Table 4, entry 18), but selectivity increased as compared to entry 18—which itself displayed already higher selectivity over VEGFR2 and TIE2 as compared to entry 10—due to an additional virtual loss of EGFR inhibition.

2.2. Improvement of cellular effects for selected kinase inhibitors

With compounds at hand displaying excellent in vitro enzyme inhibitory activities on different kinases, cellular data were acquired for selected derivatives (Table 5, down to entry 20). Somewhat disappointing results were obtained, any inhibitory activities were determined to be in the micromolar range at the most, with best EC_{50} values identified for compounds of entries 8, 10 and 12 for Aurora B or TIE2 between 2 and 5 μM—but not necessarily reflecting the most pronounced inhibition of kinases measured at the enzyme level (cf. Table 3).

Besides explanations based on different competition events within the cell (vide infra) for the unfavourable EC_{50}/IC_{50} ratios of 55–80 for the better substrates or even worse for the rest of the compounds down to entry 20, Table 5 (factor 100 to over 1000), such ratios might simply be a result of inappropriate physicochemical properties causing problems of bioavailability within the cell context. Thus the linking NH-unit between the quinazoline and arylbenzothiazole moieties was chosen for further derivatization, aiming at the removal of a protic polar group. It has been questioned in the literature whether bis(hetero)arylanilines represent a privileged structure due to exerting optimal binding properties within kinases or simply due to the simplicity of synthetic access to this core fragment.[23] For Iressa, for example, the anilinic NH is not involved in hydrogen bonding and seems to serve only as an appropriate linker guaranteeing a perfect angle between the two aromatic portions. For a series of VEGFR2 and PDGFRα inhibitors, an oxygen spacer was essential and clearly favourable over NH.[20] Consequently, this unit was exchanged by an oxygen or simply methylated for comparison. N-Methylation, however, resulted in a dramatic loss of inhibitory effects, which was least emphasized for Aurora A and B with an increase of IC_{50} values by a factor of ~30 and was most prominent at EGFR with an augmentation of IC_{50} values from 2 nM to 1400 nM (entry 22, Table 6 vs entry 13, Table 3). Replacement of the NH connector unit by oxygen generated derivatives displaying a rather similar selectivity profile as the corresponding NH substrates (cf. entries 23 and 24, Table 6 with entries 5 and 10, Table 3), even though on a reduced potency level. Inhibition of Aurora B, VEGFR3 and TIE2 became more pronounced, with IC_{50} values down to 44 nM (entry 24). The ability to inhibit EGFR was generally lost. With several examples published for successful attachment of various heterocyclic aminoalkyl units to a quinazoline adenine mimic,[14,24,25] the *N*-methylpiperazinylpropyl moiety was additionally exchanged exploratory by a pyrrolidinylpropyl, only to give a rather similar inhibitory pattern with slightly decreased potency (factor below 2.6, cf. entry 25 vs 24).

Compounds of entries 23–25 (Table 6) were likewise submitted for evaluation of inhibitory activity within cellular assays (Table 5). Sub-micromolar activities were detected on VEGFR2, TIE2 and PDGFRβ, even down to an EC_{50} of 60 nM on the former. A few cellular EC_{50} values were found to be even lower than the respective in vitro IC_{50} values, which was especially true for both PDGFRβ values (IC_{50} values in the micromolar range). As was discussed by Knight and Shokat, various settings within the cell context might allow for an outcome of cellular activity being both, either above or below an in vitro activity at an isolated enzyme.[26] Furthermore, varying binding kinetics ('drug-target residence time') for different kinases might result in very altered effects to be observed in a cellular system as compared to a mere in vitro activity assay.[27] Such notions could also explain the general lack of Aurora B inhibition even though in vitro data was quite promising, also for the O-series (e.g., entry 24: IC_{50} = 62 nM, EC_{50} >10 μM). According to these cellular results, oxygen-linked arylbenzothiazoles out of our series have now rather to be considered as VEGFR2/TIE2/PDGFRβ inhibitors. Based on the NH-linker group, good inhibitory activities on the enzymes VEGFR2 and TIE2 gave rise to only moderate to poor cellular EC_{50} values between 2.1 μM and 26 μM for entries 10, 14 and 15—which was somewhat reflecting best enzyme inhibitions observed for these compounds except for the total inactivity on Aurora kinases in the cellular context. Comparing with these results, the effect of the NH versus O exchange as linker becomes most evident, now resulting in compounds with EC_{50} values in the sub-micromolar range even down to 60 nM (entries 23–25). Most surprising, however, has been the detection of good cellular activity on PDGFRβ (entry 24) for which enzyme inhibition ranged clearly in the micromolar range for all compounds tested. The cellular inhibition profile especially of compound entry 24 seems promising, with Sunitinib being an excellent representative as it has been approved as a multi-target kinase inhibitor with main activity on VEGFR2 and PDGFRβ for the treatment of advanced renal cell carcinoma and gastrointestinal stromal tumours.[28]

Table 5
EC_{50} values (μM) for selected compounds in cellular assays

Entry	Proliferation			Angiogenesis	
	Aurora B	EGFR	PDGFRβ	VEGFR2	TIE2
8	5.0	>10	n.d.	>10	>10
10	>10	>10	n.d.	13	2.1
12	5.0	33	n.d.	>10	>10
13	>10	9.4	n.d.	>10	>10
14	>10	>10	n.d.	26	>10
15	>10	>10	n.d.	14	10
17	>10	>10	n.d.	>10	>10
19	>10	>10	n.d.	>10	>10
20	>10	>10	n.d.	>10	>10
23	>10	>10	n.d.	0.78	0.30
24	>10	n.d.	0.17	0.06	0.54
25	>10	n.d.	2	0.80	0.14

2.3. Into SAR explanations

2.3.1. Influence of the gatekeeper residue

For a general analysis of SAR attained for the (aminoaryl)benzothiazole quinazoline derivatives, a comparison of binding modes with those of Iressa, Tarceva[29] and the AstraZeneca compound **24**[24] (Fig. 1) seemed reasonable, as their structural similarity should result in similar binding—and the binding modes of the latter two compounds have been discussed extensively by Liao.[8] Based on the 7′-attachment of the solubility enhancer at the quinazoline unit in compound **24**, which resulted in best inhibitory potency in our series as well, this Aurora A ligand was assumed to cover identical areas of the binding pocket, with the piperidine penetrating into E_0 and the arylcarboxamide extension occupying the intersection of BP-I and BP-II. The same latter orientation was expected to be adopted by the benzothiazole moiety of our series. Binding of the three reference compounds as depicted in Figure 1 into EGFR (Iressa, Tarceva) or Aurora A (for **24**), as visualized by crystal structures 2ITY, 1M17 and 2C6E (PDB), will significantly be influenced by the dihedral angle between the quinazoline plain and the aromatic ring connected to the former via the anilinic NH linker, as the anilinic aromatic ring is positioned in close proximity to the gatekeeper residue (the latter amino acid is shown in spheres). According to a statistic analysis of such an angle for other *N*-(hetero)arylaniline-kinase-inhibitors by Aronov et al.,[23] it is adjusted most frequently to around 10–50° (median angle 23°)—and

Table 6
In vitro IC_{50} values (μM) on selected kinases out of a panel of 16

	Entry	Z	R^1	R^2	Proliferation				Angiogenesis		
					Aurora A	Aurora B	EGFR	PDGFRβ	VEGFR2	VEGFR3	TIE2
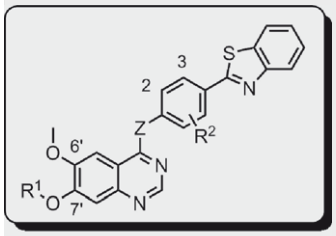	22	NMe	X^1	3-OMe	3.300	8.000	1.400	>10	>10	>10	>10
	23	O	X^1	2-F	0.220	0.130	>10	6.100	0.420	0.190	0.088
	24	O	X^1	H	0.082	0.063	>10	3.500	0.147	0.121	0.044
	25	O	X^2	H	0.170	0.162	>10	7.700	0.350	0.140	0.072
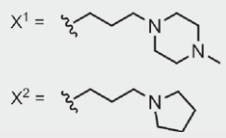											
	0.021-0.1 μM										
	0.101-0.35 μM										

was found to be around 45° for Tarceva and compound **24** (even though with opposite sign) and 55° for Iressa. The smaller this angle gets the more pronounced the overall π-overlap becomes, furnishing the linking NH with increasing sp^2 hybridization and connecting both aromatic regions. The general variations of inhibitory potencies observed for our series of compounds might be explained by analyzing the size of the gatekeeper residue of different kinases (Table 2) along with influences of substitution pattern at the central aromatic and choice of the linker unit (Z = NH vs O vs NMe; Fig. 3) on the dihedral angle. Protein sequence alignment of the kinase domain of all 17 kinases of the screening set validated by cross-referencing the gatekeeper residues deduced by this approach with literature data[30] allowed for a classification by increasing size (1 to 4) according to its estimated size Thr ~ Val (1) < Leu ~ Ile (2) < Met (3) < Phe (4). When comparing the size of gatekeeper residues for those kinases on which our compounds displayed in vitro IC_{50} values below 300 nM, it is striking that larger residues (size 3 and 4) were not tolerated at all, not one IC_{50} value was detected below 300 nM on respective kinases (including InsR). Best enzymatic inhibition, on the other hand, was found on Aurora A and B, TIE2, and EGFR/ErbB2 and most promising cellular data on PDGFRβ, VEGFR2 and again TIE2, with all of these kinases possessing gatekeeper residues of sizes 1 or 2.

With further substituents placed on the anilinic portion of the arylbenzothiazole unit, not only the size but also the constitution of the gatekeeper residue seems to be of importance. As can be seen from the crystal structures in Figure 1, two different general orientations of the central aromatic can be adopted, either positioning a *meta*-substituent (relative to the anilinic NH) 'above' the gatekeeper residue (Iressa, Tarceva; dihedral angle +45–55°) or 'underneath' the gatekeeper residue (compound **24**; dihedral angle −45°)—or alternatively within the latter mode towards the conserved lysine residue present in the phosphate binding site (e.g., K745 in EGFR, K162 in Aurora A or K855 in TIE2). For kinases of the ErbB family, the threonine gatekeeper offers an additional hydroxyl group for polar interactions, which can theoretically be addressed by either binding mode. Visualized by a manual docking experiment of the 3-methoxy substituted derivative of entry 4 (Table 1), positions of said threonine hydroxyl group in either orientation (2ITY or 1M17) allow indeed for such a hydrogen bonding in EGFR and ErbB2 either from 'above' or from 'underneath' (Fig. 2; distances between 2.7 and 3.6 Å). This cannot be realized with leucine as gatekeeper residue (Aurora kinases), consequently resulting in excellent nanomolar in vitro IC_{50} values for such 3-OMe derivatives (entries 4, 13, Tables 1 and 3; and entry 7, Table S1, Supplementary data) on the ErbB kinases paralleled by a clear diminution of inhibition of Aurora kinases—still moderate IC_{50} values of 120 and 300 nM (Aurora A and B, respectively) as encountered for compound of entry 13 might be based on a flip of the central aromatic allowing for a certain binding involvement of the conserved lysine to the 3-methoxy group.

2.3.2. Analysis of the dihedral angle

A second approach for explaining different effects of substituent positions at the central aromatic ring or exchange of the linking unit Z on inhibition was based on the intrinsic energy profile of the molecules in dependence on the dihedral angle between the quinazoline plain and the aromatic ring of the arylbenzothiazole unit (Fig. 3). Such an influence was calculated using density functional theory (DFT; B3LYP/6-31G**) for several derivatives, by calculating the total energy of a molecule adjusting the dihedral angle between 0° and 90° in 10° steps and monitoring the energy difference towards the respective minimum value of such a sequence for a given molecule. Within the Z = NH series (unsubstituted vs 2-OMe vs 3-OMe) the energetic minimum was always around a dihedral angle of 0–10°, which is achievable for the 2-OMe derivative if the substituent is directed towards the NH bond, stabilized by an intramolecular hydrogen bond. When increasing the dihedral angle, sp^2 hybridization of the anilinic nitrogen becomes increasingly perturbed by sp^3 participation, which is resulting in very different effects within the 3-OMe versus the 2-OMe derivative. Within the former, the anilinic nitrogen is keeping up as high a conjugation with the quinazoline moiety as possible, the benzothiazole itself starts to rotate out of conjugation within the arylbenzothiazole portion (aryl vs benzothiazole). For the 2-OMe derivative, the NH bond rather attempts to stay within the arylbenzothiazole plain within reach of an intramolecular hydrogen bond, with the arylbenzothiazole plain itself not experiencing any distortion in this case. Consequently, both series (2- vs 3-substituted) seem to develop a significantly different spatial demand with increasing dihedral angle, which might serve as an explanation for the different selectivity profiles identified for the two series with regard to non-threonine gatekeeper containing kinases.

As to the nature of the linker unit, it was hypothesized for a set of VEGFR2 inhibitors that the loss of affinity for their NH- versus O-series might be a result of different hybridization of the linker atom (rather sp^2 for the nitrogen vs sp^3 for the oxygen) translating into different orientations of the two aromatic units.[20] This, however, would not reflect our findings within the enzyme assays

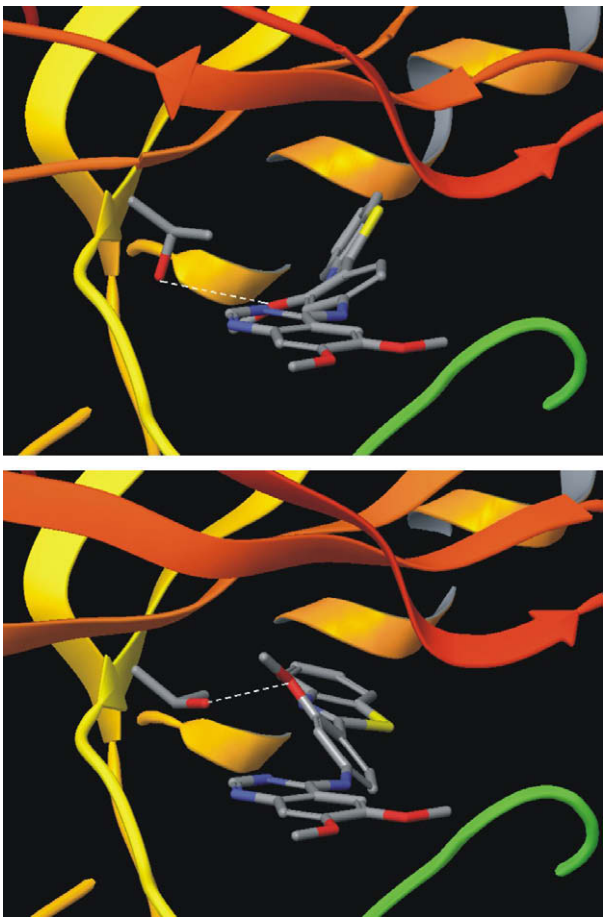

Figure 2. Positioning of compound entry 4 (Table 1) into the crystal structure of EGFR taken from 2ITY (top) and 1M17 (bottom): quinazoline part was superimposed with the corresponding unit of Iressa and Tarceva, respectively, dihedral angles between central aryl and quinazoline as well as between central aryl and benzothiazole were adjusted according to DFT calculations and statistic evaluations (cf. Section 2.3.2, around 40° for the former). Positioning of the gatekeeper threonine residue (sticks) is shown as present in the crystal structures. Possible hydrogen bonding from the 3-OMe group of the ligand towards the threonine hydroxyl group in a favourable distance (around 3 Å) are highlighted by a dotted line.

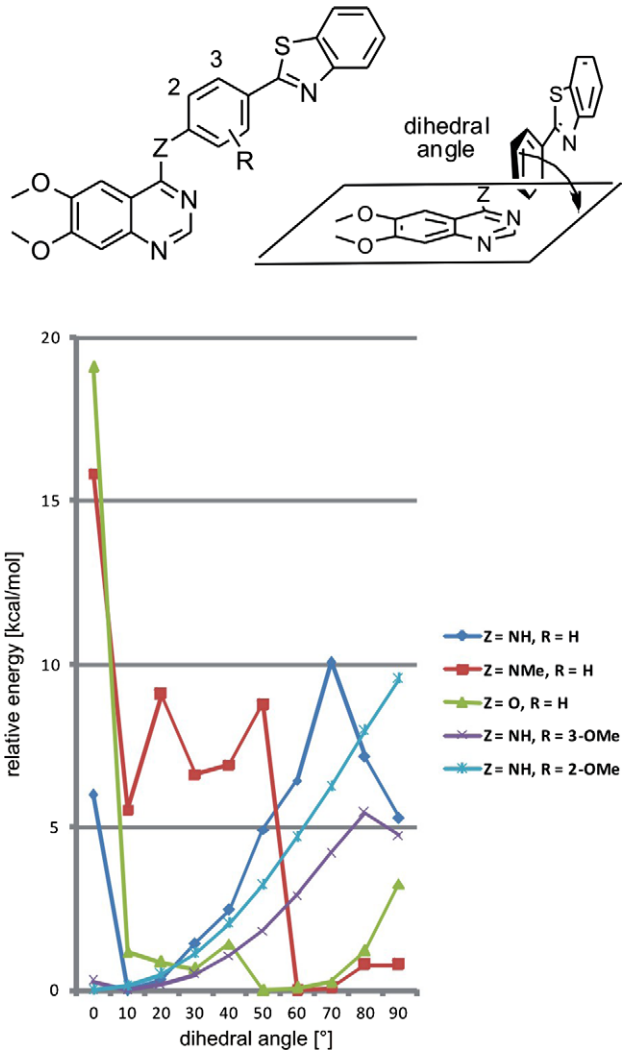

Figure 3. Influence of linker and substituent choice on the relative energy content in dependence on the dihedral angle within the molecule (DFT; B3LYP/6-31G**). Graphs display the energy difference towards the respective energy minimum in dependence on the dihedral angle for each compound evaluated.

(NH-series slightly favourable over the respective O-derivatives, even on VEGFR2). For comparison of Z = NH vs Z = NMe, hybridization of the nitrogen might be a decisive factor, as for a dihedral angle of 0°, complete sp^2 hybridization was identified by DFT calculations for Z = NH, whereas the NMe derivative has to endure certain molecular constraints to circumvent steric hindrance by the additional methyl group resulting in a small but distinct sp^3 character. Increasing the dihedral angle, steric interaction is minimized, which is, however, paralleled by an increasing loss of sp^2 character due to the diminution of conjugation. These effects result in a most preferable minimum structure with a dihedral angle of 10° for the NH variant, whereas the NMe derivative reaches its minimum not before an angle of 60°. With oxygen being more prone to sp^3 hybridization, no clean sp^2 hybrid is present even at a dihedral angle of 0°, resulting in a certain bent structure of the molecule. With a total conjugation factor thus being less emphasized within the O-series, avoiding steric hindrance within the molecule becomes the decisive factor, and the energetic minimum is reached around a dihedral angle of 50°. Regarding the assumption that a best fit into the enzyme pocket might be achieved with dihedral angles between 10° and 50° (based on the statistical evaluation of literature data, vide supra), allowing for the arylbenzothiazole to pass beside the gatekeeper residue into the back cleft, the energy difference towards their energetic minimum for Z = O and NH is rather similar and low (cf. energy plot, Fig. 3) in this range of the angle, whereas it is constantly on a higher level for Z = NMe, thus rendering it rather difficult for the molecule to adopt such an angle: This might be a plausible explanation for the virtual loss of potency for the latter.

2.4. Selectivity profiling: panel of 252 kinases

Having identified compounds now also displaying cellular activity, a more profound selectivity profile was determined for the three oxygen-bridged compounds of entries 23–25. Their inhibitory activity on a panel of 252 kinases was investigated at compound concentrations of 0.1, 1.0 and 10 μM. For a complete list of test results, please refer to the Supplementary data. With a cut-off chosen at 30% inhibition or below at 1 μM compound concentration—which would translate into IC_{50} values around or above approximately 5 μM—rather similar profiles were attained for all three compounds, resulting in 18–25 kinases being hit simultaneously, with only around 10 kinases being potentially inhibited in the submicromolar range (Fig. 4). Highest inhibition values at 0.1 μM were identified for all three compounds on Aurora B, C

and TIE2 with values between 47% and 62%. Furthermore, BRK, MERTK, SAK and VEGFR3 were usually privileged targets for inhibition by two of the three compounds evaluated. With the Aurora kinases playing a crucial role in regulation of mitosis,[2,7] TIE2 and VEGFRs being linked to tumour angiogenesis,[3] BRK being described to potentiate EGF-induced proliferation in breast cancer cells,[31] MERTK influencing cell survival signaling[32] and SAK inhibitors being discussed as potential apoptosis-inducing anticancer drugs,[33] the clearly confined selectivity profiles determined for our compounds of entries 23–25 might offer a chance to tackle appropriately selected cancer types by addressing a few different mechanisms in tumour progression, which might result in high efficacy in in vivo models. However, as was already evident from our results depicted in Section 2.2, inhibitory activity in enzyme assays does not necessarily translate into activity in a cellular context, which was especially true for Aurora B in a negative and for PDGFRβ in a positive sense. Consequently, a thorough screening of cellular activity followed by an educated selection of appropriate cancer cell lines for a further evaluation of these compounds has to be initiated now in order to avoid missed opportunities or an incorrect focus based on enzymatic data. Furthermore, MERTK inhibition has to be monitored with regard to (reversible) retinal degeneration in long-term treatment for a definition of a possible therapeutic window.[32]

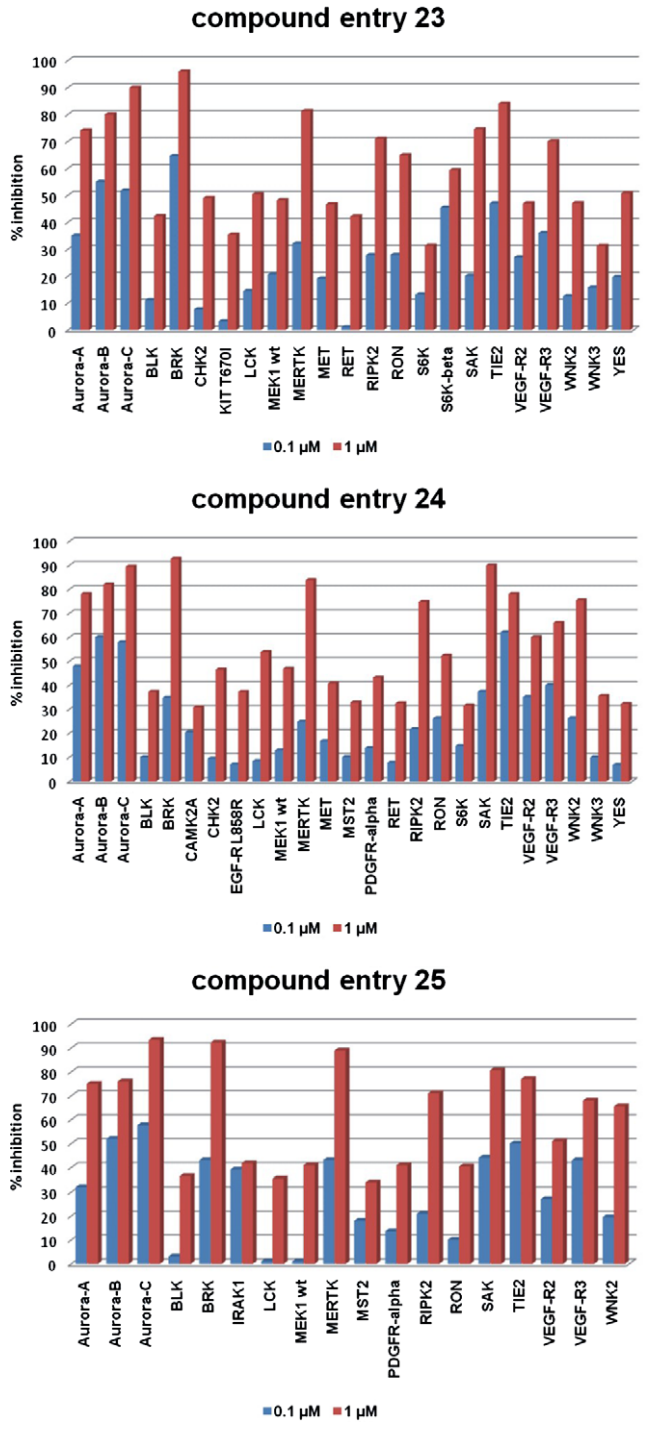

Figure 4. Profile of kinase inhibition for compounds entry 23–25 at 0.1 and 1.0 µM compound concentrations with inhibitions above 30% at 1 µM out of a panel of 252 kinases.

3. Conclusion

With introduction of the di-(hetero)arylether series, a lead scaffold has been identified, now resulting in excellent EC_{50}/IC_{50} ratios on selected kinases, with enzymatic IC_{50} values below 100 nM and cellular EC_{50} values between 60 and 800 nM (entries 23–25). Best enzyme inhibitions for these compounds were detected on Aurora and VEGFR kinases as well as on TIE2, whereas the corresponding NH-derivatives displayed excellent inhibitory potential on EGFR/ErbB2 in several cases, with IC_{50} values even below 10 nM. For Aurora and EGFR kinases, such in vitro potencies could not translate into good activities in the respective cellular assay, whereas on PDGFRβ, VEGFR2 and TIE2, good activities were detected. In general, all these compounds did not show significant in vitro inhibition of InsR, with IC_{50} values >3 µM in all cases and >10 µM for most derivatives.

Several possibilities for tuning selectivity, targeted kinase groups and solubility have been demonstrated by variation of substituents at the central aromatic or the distal ring on the benzothiazole moiety and attachments of solubilizing groups in 6′- or 7′-position of the quinazoline, with further options by varying such a group itself. An exchange of NH within the *N*-(hetero)arylaniline by oxygen resulted in a drastic increase in cellular activity. Possible explanations for SAR trends have been elaborated applying computational tools, which should allow for a most stringent further lead optimization.

4. Experimental

4.1. Chemistry

Preparative TLC: Merck PLC plates, Silica Gel 60 F_{254}, coating thickness 0.5 mm, 1.0 mm or 2.0 mm. NMR spectra: Bruker Avance 300 MHz, recorded at room temperature. The chemical shifts are given in ppm, the residual solvent peak was used as an internal standard ($CDCl_3$: δ 7.26; CD_3OD: δ 3.31; DMSO-d_6: δ 2.49). Analytical LC/ESIMS: Waters 2700 Autosampler; Waters 1525 Multisolvent Delivery System; column: Chromolith Fast Gradient C18, 50 × 2 mm (Merck) with stainless steel 2 µm prefilter. Waters Micromass ZQ single quadrupol mass spectrometer with electrospray source. MS method: MS5_30minPM-80-800-35 V; positive/negative ion mode scanning. Preparative HPLC/ESIMS: Waters 600 Multisolvent Delivery System with peparative pump heads; 2 mL or 5 mL sample loop; column: Waters X-Terra RP18, 7 µm, 19 × 150 mm with X-Terra RP18 guard cartridge 7 µm, 19 × 10 mm; flow rate: 20 mL/min; or YMC ODS-A, 120 Å, 40 × 150 mm with X-Terra RP18 guard cartridge 7 µm, 19 × 10 mm; flow rate: 50 mL/min. Make-up solvent: MeCN–H_2O–HCO_2H 80:20:0.05 (v/v/v). All reagents and building blocks were commercially available if not indicated otherwise. Reactions were not optimized for maximum yields. The synthesis of compounds **2**–**9**,

11–**19**, 2′-(4-aminophenyl)benzothiazoles **20** and 4-(benzothiazol-2′-yl)phenols **21** is described in the Supplementary data of this article.

4.1.1. General procedure: synthesis of N-substituted 2′-(4-aminoaryl)benzothiazoles 22

To a mixture of the respective 4-chloroquinazoline **8** or **17** (0.130 mmol) and a suitable 2′-(4-aminophenyl)benzothiazole **20** (0.143 mmol) in ethylene glycol (1.2 mL) was added 4 M HCl in dioxane (0.260 mmol), and the sealed vial was heated for 3 h at the indicated temperature. *Purification method I:* The reaction mixture was partitioned between satd aq $NaHCO_3$/brine 1:3 (100 mL) and $CHCl_3$ (100 mL, then 2 × 50 mL). Combined organic phases were re-extracted once against 50 mL brine and dried over $MgSO_4$. Product was crystallized from $CHCl_3$/Et_2O (Ia) or acetone/Et_2O (Ib). *Purification method II:* The reaction mixture was purified by preparative HPLC. Eluent A: 0.1% aqueous HCO_2H (IIa) or water (IIb); eluent B: MeCN. Gradient: 95% A + 5% B to 100% B linear within 3.80 min, then isocratic for 0.20 min, then back to 95% A + 5% B within 0.07 min, then isocratic for 0.23 min; flow: 0.6 mL/min and 1.2 mL/min.

4.1.1.1. *N*-[4-(Benzo[*d*]thiazol-2″-yl)phenyl]-6′-methoxy-7′-[3-(4-methylpiperazin-1-yl)propoxy]quinazolin-4′-amine (Table 3, entry 5). From **8** and 2′-(4-aminophenyl)benzothiazole at 110 °C. Purification method Ia. Yield: 74%. ^{1}H NMR (300 MHz, CD_3OD): δ 2.15 (m_c, 2H), 2.39 (s, 3H), 2.64 (br s, 8H), 2.69 (t, J = 7.4 Hz, 2H), 4.08 (s, 3H), 4.26 (t, J = 6.2 Hz, 2H), 7.20 (s, 1H), 7.44 (td, J = 7.6, 1.1 Hz, 1H), 7.54 (td, J = 7.6, 1.1 Hz, 1H), 7.79 (s, 1H), 7.99 (d, J = 7.6 Hz, 1H), 8.04 (m, 3H), 8.13 (d, J = 8.8 Hz, 2H), 8.55 (s, 1H); LC/(+)ESIMS (m/z): 541 [$(M+1)^+$, 20%], 401 [47%], 271 [$(M+2)^{2+}$, 100%], 141 [77%]; LC/(−)ESIMS (m/z): 539 [$(M-1)^-$, 100%].

For a description of the synthesis and characterization data of the remaining **22** analogs, please see the Supplementary data of this article.

4.1.2. General procedure: synthesis of O-substituted 2′-(4-hydroxyaryl)benzothiazoles 23[20]

To a solution of the respective 4-(benzothiazol-2′-yl)phenol **21** (0.096 mmol) in DMSO (2 mL) was added NaH (0.12 mmol, 60% dispersion in mineral oil) at 0 °C, and the mixture was stirred for 10 min at room temperature. The respective 4-chloroquinazoline **8** or **9** (0.08 mmol) was added, and the mixture was heated at 130 °C for 12 h. The products were purified by preparative HPLC. Eluent A: water; eluent B: MeCN. Gradient: 95% A + 5% B to 100% B linear within 3.80 min, then isocratic for 0.20 min, then back to 95% A + 5% B within 0.07 min, then isocratic for 0.23 min; flow: 0.6 mL/min and 1.2 mL/min.

4.1.2.1. *O*-[4-(Benzo[*d*]thiazol-2″-yl)-2-fluorophenyl]-6′-methoxy-7′-[3-(4-methylpiperazin-1-yl)propoxy]quinazolin-4′-hydroxide (Table 6, entry 23). From **8** and 4-(benzothiazol-2′-yl)-2-fluorophenol. Yield: 22%. ^{1}H NMR (300 MHz, $CDCl_3$): δ 2.15 (m_c, 2H), 2.49 (s, 3H), 2.67 (t, J = 7.0 Hz, 2H), 2.75 (br s, 8H), 4.05 (s, 3H), 4.28 (t, J = 6.4 Hz, 2H), 7.36 (s, 1H), 7.41 (ddd, J = 8.3, 7.3, 1.2 Hz, 1H), 7.46 (d, J = 8.4 Hz, 1H), 7.52 (ddd, J = 8.3, 7.3, 1.2 Hz, 1H), 7.56 (s, 1H), 7.92 (d, J = 8.3 Hz, 1H), 7.96 (ddd, J = 8.4, 2.0, 1.0 Hz, 1H), 8.04 (dd, J = 10.7, 2.0 Hz, 1H), 8.09 (d, J = 8.3 Hz, 1H), 8.61 (s, 1H); LC/(+)ESIMS (m/z): 560 [$(M+1)^+$, 96%], 420 [29%], 280.5 [$(M+2)^{2+}$, 27%], 141 [100%].

4.1.2.2. *O*-[4-(Benzo[*d*]thiazol-2″-yl)phenyl]-6′-methoxy-7′-[3-(4-methylpiperazin-1-yl)propoxy]quinazolin-4′-hydroxide (Table 6, entry 24). From **8** and 4-(benzothiazol-2′-yl)phenol. Yield: 16%. ^{1}H NMR (300 MHz, $CDCl_3$): δ 2.15 (m_c, 2H), 2.54 (s, 3H), 2.69 (t, J = 7.0 Hz, 2H), 2.80 (br, 8H), 4.05 (s, 3H), 4.28 (t, J = 6.4 Hz, 2H), 7.35 (s, 1H), 7.40 (td, J = 7.9, 1.2 Hz, 1H), 7.41 (d, J = 8.8 Hz, 2H), 7.50 (td, J = 7.9, 1.2 Hz, 1H), 7.55 (s, 1H), 7.92 (d, J = 7.9 Hz, 1H), 8.09 (d, J = 7.9 Hz, 1H), 8.22 (d, J = 8.8 Hz, 2H), 8.63 (s, 1H); LC/(+)ESIMS (m/z): 542 [$(M+1)^+$, 54%], 402 [93%], 271.5 [$(M+2)^{2+}$, 36%], 141 [100%].

4.1.2.3. *O*-[4-(Benzo[*d*]thiazol-2″-yl)phenyl]-6′-methoxy-7′-[3-(pyrrolidin-1-yl)propoxy]quinazolin-4′-hydroxide (Table 6, entry 25). From **9** and 4-(benzothiazol-2′-yl)phenol. Yield: 21%. ^{1}H NMR (300 MHz, DMSO-d_6): δ 1.70 (m_c, 4H), 2.00 (m_c, 2H), 2.47 (br s, 4H), 2.58 (t, J = 7.1 Hz, 2H), 4.00 (s, 3H), 4.27 (t, J = 6.4 Hz, 2H), 7.40 (s, 1H), 7.49 (ddd, J = 8.1, 6.9, 1.2 Hz, 1H), 7.55 (d, J = 8.7 Hz, 2H), 7.57 (ddd, J = 7.8, 6.9, 1.3 Hz, 1H), 7.60 (s, 1H), 8.09 (d, J = 8.1 Hz, 1H), 8.18 (d, J = 7.8 Hz, 1H), 8.22 (d, J = 8.7 Hz, 2H), 8.58 (s, 1H); LC/(+)ESIMS (m/z): 513 [$(M+1)^+$, 100%], 402 [10%], 257 [$(M+2)^{2+}$, 56%], 112 [33%].

4.2. Biological assay systems

4.2.1. In vitro protein kinase activity assays[12]

A radiometric protein kinase assay was used for measuring in vitro protein kinase activity. All kinase assays were performed in 96-well FlashPlates™ from Perkin Elmer/NEN (Boston, MA, USA) in a 50 μL reaction volume. The assay reaction cocktail included 60 mM HEPES-NaOH, pH 7.5, 3 mM $MgCl_2$, 3 mM $MnCl_2$, 3 μM Na-orthovanadate, 1.2 mM DTT, 50 μg/mL polyethylene glycol 20000 and 1 μM [γ-^{33}P]-ATP that equalled approximately 5 × 10^5 cpm per well, recombinant protein kinase (10–200 ng per well) and, depending on the kinase, the following substrate proteins: Casein (PLK1), GSK3(14-27) peptide (AKT1), histone H1 (CDK2/CycA), Rb-CTF (CDK4/CycD1), poly(Ala,Glu,Lys,Tyr)$_{6:2:5:1}$ (InsR, PDGFRβ), poly(Glu,Tyr)$_{4:1}$ (EGFR, EphB4, ErbB2, FAK, IGF1R, TIE2, Src, VEGFR2, VEGFR3) and tetra(LRRWSLG) peptide (Aurora A, Aurora B). Reaction was performed at 30 °C for 80 min and stopped by addition of 50 μL of 2% (v/v) aq H_3PO_4. After washing, incorporation of radioactive $^{33}P_i$ was measured with a microplate scintillation counter (Microbeta Trilux, Wallac). IC_{50} values were determined by single-point measurements at 10 compound concentrations ranging from 3 nM to 100 μM in half-logarithmic steps and were calculated using the program Quattro Workflow 2 (Quattro Research GmbH, Munich, Germany; http://www.quattro-research.com). The fitting model for the IC_{50} determinations was 'Sigmoidal response (variable slope)' with parameters 'top' fixed at 100% and 'bottom' at 0%.

4.2.2. Cellular endoreduplication assay for Aurora B

Cellular inhibitory activity of compounds on Aurora B was determined in a FACS-based endoreduplication assay. The assay is based on the propidium iodide (PI) fluorescence determination as a measure for the DNA amount in HCT116 colon carcinoma cells increasing upon endoreduplication. In brief, cells were cultivated for 72 h in the presence of different compound concentrations. Subsequently the percentage of endoreduplicated cells yielding a PI fluorescence signal exceeding that of cells with a chromosome content of 2n was determined. Upon plotting the percentage of endoreduplicated cells against the compound concentration a sigmoidal regression curve and a corresponding EC_{50} value was determined using the program Prism 4.03 (GraphPad Software, San Diego, CA, USA; www.graphpad.com). For each EC_{50} curve, five compound concentrations were measured once ranging from 1 nM to 10 μM as a logarithmic serial.

4.2.3. Cellular phosphorylation assays for EGFR, PDGFRβ, VEGFR2 and TIE2

Cellular activity on the receptor tyrosine kinases (RTK) EGFR, PDGFRβ, VEGFR2 and TIE2 was tested by determining the inhibition of the autophosphorylation of these receptors. Test compounds

were applied to cells expressing the respective RTKs. Stimulation of cells resulted in maximal autophosphorylation in control cells (high control) and decreased phosphorylation levels in cells bearing successfully inhibited RTKs. Subsequently, cells were lysed using a standard lysis buffer preserving the distinct phosphoprotein levels. RTK-phosphorylation was quantified via sandwich ELISA using receptor-specific capture antibodies and a phosphotyrosine antibody.

Sigmoidal inhibitor curves based on relative inhibition compared with phosphorylation levels under high control conditions were generated and allowed the determination of EC_{50} values for each test compound. For each EC_{50} curve, nine compound concentrations were measured in duplicate ranging from 1 nM to 10 μM as a half-logarithmic serial.

Acknowledgement

Scientific input by Dr. Christophe Henry was highly appreciated.

Supplementary data

Supplementary data (table with residual activities of three compounds on a 252 protein kinase panel, Table S1 for quinazoline derivatives with a solubilizing group being attached to 6′-position, and details for the synthesis of 2′-(4-aminophenyl)benzothiazoles **20**, 4-(benzothiazol-2′-yl)phenols **21**, compounds **2–9**, **11–19** and **22**) associated with this article can be found, in the online version, at doi:10.1016/j.bmc.2009.07.047.

References and notes

1. Tasler, S.; Müller, O.; Wieber, T.; Herz, T.; Krauss, R.; Totzke, F.; Kubbutat, M. H. G.; Schächtele, C. *Bioorg. Med. Chem. Lett.* **2009**, *19*, 1349.
2. Harrington, E. A.; Bebbington, D.; Moore, J.; Rasmussen, R. K.; Ajose-Adeogun, A. O.; Nakayama, T.; Graham, J. A.; Demur, C.; Hercend, T.; Diu-Hercend, A.; Su, M.; Golec, J. M. C.; Miller, K. M. *Nature Med.* **2004**, *10*, 262.
3. (a) Shchemelinin, I.; Sefc, L.; Necas, E. *Folia Biolog.* **2006**, *52*, 137; (b) Blume-Jensen, P.; Hunter, T. *Nature* **2001**, *411*, 355.
4. Muhsin, M.; Graham, J.; Kirkpatrick, P. *Nat. Rev. Drug Disc.* **2003**, *2*, 515.
5. Dancey, J.; Sausville, E. A. *Nat. Rev. Drug Disc.* **2003**, *2*, 296.
6. (a) Normanno, N.; Bianco, C.; Strizzi, L.; Mancino, M.; Maiello, M. R.; De Luca, A.; Caponigro, F.; Salomon, D. S. *Curr. Drug Targets* **2005**, *6*, 243; (b) Albanell, J.; Gascon, P. *Curr. Drug Targets* **2005**, *6*, 259.
7. Blagden, S.; de Bono, J. *Curr. Drug Targets* **2005**, *6*, 325.
8. Liao, J. J.-L. *J. Med. Chem.* **2007**, *50*, 409.
9. (a) Stadler, W. M. *J. Clin. Oncol.* **2006**, *24*, 4; (b) Daub, H.; Specht, K.; Ullrich, A. *Nat. Rev. Drug Disc.* **2004**, *3*, 1001.
10. Bridges, A. J. *Chem. Rev.* **2001**, *101*, 2541.
11. Underiner, T. L.; Ruggeri, B.; Gingrich, D. E. *Curr. Med. Chem.* **2004**, *11*, 731.
12. For a list of kinases for which binding assays have been established, see www.proqinase.com; Sachsenmaier, C.; Schaechtele, C. *BioTechniques* **2002**, *33*, 101.
13. Barker, A. J.; Gibson, K. H.; Grundy, W.; Godfrey, A. A.; Barlow, J. J.; Healy, M. P.; Woodburn, J. R.; Ashton, S. E.; Curry, B. J.; Scarlett, L.; Henthorn, L.; Richards, L. *Bioorg. Med. Chem. Lett.* **2001**, *11*, 1911.
14. Pandey, A.; Volkots, D. L.; Seroogy, J. M.; Rose, J. W.; Yu, J.-C.; Lambing, J. L.; Hutchaleelaha, A.; Hollenbach, S. J.; Abe, K.; Giese, N. A.; Scarborough, R. M. *J. Med. Chem.* **2002**, *45*, 3772.
15. Berger, D.; Dutia, M.; Powell, D.; Wissner, A.; DeMorin, F.; Raifeld, Y.; Weber, J.; Boschelli, F. *Bioorg. Med. Chem. Lett.* **2002**, *12*, 2989.
16. (a) Barge, A. W.O. Patent 2004/043472 A1, 2004; *Chem. Abstr.* **2004**, *141*, 1220; (b) Plé, P. W.O. Patent 2004/041829 A1, 2004; *Chem. Abstr.* **2004**, *140*, 423698.
17. (a) Meyer, J. F.; Wagner, E. C. *J. Org. Chem.* **1943**, *8*, 239; (b) Alexandre, F. R.; Berecibar, A.; Besson, T. *Tetrahedron Lett.* **2002**, *43*, 3911.
18. Kolloff, H. G.; Hunter, J. H.; Woodruff, E. H.; Moffett, R. B. *J. Am. Chem. Soc.* **1948**, *70*, 3862.
19. For similar reaction conditions (HCl, *i*-PrOH, Δ), see: Plé, P. A.; Green, T. P.; Hennequin, L. F.; Curwen, J.; Fennell, M.; Allen, J.; Lambert-van der Brempt, C.; Costello, G. *J. Med. Chem.* **2004**, *47*, 871.
20. Kubo, K.; Shimizu, T.; Ohyama, S.-i.; Murooka, H.; Iwai, A.; Nakamaru, K.; Hasegawa, K.; Kobayashi, Y.; Takahashi, N.; Takahashi, K.; Kato, S.; Izawa, T.; Isoe, T. *J. Med. Chem.* **2005**, *48*, 1359.
21. (a) Kashiyama, E.; Hutchinson, I.; Chua, M.-S.; Stinson, S. F.; Phillips, L. R.; Kaur, G.; Sausville, E. A.; Bradshaw, T. D.; Westwell, A. D.; Stevens, M. F. G. *J. Med. Chem.* **1999**, *42*, 4172; (b) Hutchinson, I.; Chua, M.-S.; Browne, H. L.; Trapani, V.; Bradshaw, T. D.; Westwell, A. D.; Stevens, M. F. G. *J. Med. Chem.* **2001**, *44*, 1446; (c) Phoon, C. W.; Ng, P. Y.; Ting, A. E.; Yeo, S. L.; Sim, M. M. *Bioorg. Med. Chem. Lett.* **2001**, *11*, 1647. For additional literature on 2′-arylbenzothiazole syntheses, see ref. S1, Supplementary data.
22. Barbacci, E. G.; Pustilnik, L. R.; Rossi, A. M. K.; Emerson, E.; Miller, P. E.; Boscoe, B. P.; Cox, E. D.; Iwata, K. K.; Jani, J. P.; Provoncha, K.; Kath, J. C.; Liu, Z.; Moyer, J. D. *Cancer Res.* **2003**, *63*, 4450. Additionally, a sequence alignment was performed and compared with the pocket as deduced from the crystal structure of Iressa, PDB code 2ITY.
23. Aronov, A. M.; McClain, B.; Moody, C. S.; Murcko, M. A. *J. Med. Chem.* **2008**, *51*, 1214.
24. Heron, N. M.; Anderson, M.; Blowers, D. P.; Breed, J.; Eden, J. M.; Green, S.; Hill, G. B.; Johnson, T.; Jung, F. H.; McMiken, H. H. J.; Mortlock, A. A.; Pannifer, A. D.; Pauptit, R. A.; Pink, J.; Roberts, N. J.; Rowsell, S. *Bioorg. Med. Chem. Lett.* **2006**, *16*, 1320.
25. (a) Hennequin, L. F.; Stokes, E. S. E.; Thomas, A. P.; Johnstone, C.; Plé, P. A.; Ogilvie, D. J.; Dukes, M.; Wedge, S. R.; Kendrew, J.; Curwen, J. O. *J. Med. Chem.* **2002**, *45*, 1300; (b) Jung, F. H.; Pasquet, G.; Lambert-van der Brempt, C.; Lohmann, J.-J. M.; Warin, N.; Renaud, F.; Germain, H.; De Savi, C.; Roberts, N.; Johnson, T.; Dousson, C.; Hill, G. B.; Mortlock, A. A.; Heron, N.; Wilkinson, R. W.; Wedge, S. R.; Heaton, S. P.; Odedra, R.; Keen, N. J.; Green, S.; Brown, E.; Thompson, K.; Brightwell, S. *J. Med. Chem.* **2006**, *49*, 955; (c) Hennequin, L. F.; Allen, J.; Breed, J.; Curwen, J.; Fennell, M.; Green, T. P.; Lambert-van der Brempt, C.; Morgentin, R.; Norman, R. A.; Olivier, A.; Otterbein, L.; Plé, P. A.; Warin, N.; Costello, G. *J. Med. Chem.* **2006**, *49*, 6465.
26. Knight, Z. A.; Shokat, K. M. *Chem. Biol.* **2005**, *12*, 621; cf. also (a) Schäfer, M.; Egner, U. *Anti-Inflamm. Anti-Allergy Agents Med. Chem.* **2007**, *6*, 5; (b) Bain, J.; Plater, L.; Elliott, M.; Shpiro, N.; Hastie, C. J.; McLauchlan, H.; Klevernic, I.; Arthur, J. S. C.; Alessi, D. R.; Cohen, P. *Biochem. J.* **2007**, *408*, 297; (c) Diller, D. J.; Li, R. *J. Med. Chem.* **2003**, *46*, 4638.
27. Copeland, R. A.; Pompliano, D. L.; Meek, T. D. *Nat. Rev. Drug Disc.* **2006**, *5*, 730.
28. (a) La Porta, C. A. M. *Curr. Drug Targets* **2004**, *5*, 347; (b) Sun, L.; Liang, C.; Shirazian, S.; Zhou, Y.; Miller, T.; Cui, J.; Fukuda, J. Y.; Chu, J.-Y.; Nematalla, A.; Wang, X.; Chen, H.; Sistla, A.; Luu, T. C.; Tang, F.; Wei, J.; Tang, C. *J. Med. Chem.* **2003**, *46*, 1116; (c) Faivre, S.; Demetri, G.; Sargent, W.; Raymond, E. *Nat. Rev. Drug Disc.* **2007**, *6*, 734.
29. (a) Stamos, J.; Sliwkowski, M. X.; Eigenbrot, C. *J. Biol. Chem.* **2002**, *277*, 46265; (b) Dowell, J.; Minna, J. D.; Kirkpatrick, P. *Nat. Rev. Drug Disc.* **2005**, *4*, S14.
30. (a) Gunby, R. H.; Ahmed, S.; Sottocornola, R.; Gasser, M.; Redaelli, S.; Mologni, L.; Tartari, C. J.; Belloni, V.; Gambacorti-Passerini, C.; Scapozza, L. *J. Med. Chem.* **2006**, *49*, 5759; (b) Blencke, S.; Zech, B.; Engkvist, O.; Greff, Z.; Örfi, L.; Horvath, Z.; Keri, G.; Ullrich, A.; Daub, H. *Chem. Biol.* **2004**, *11*, 691; (c) Böhmer, F. D.; Karagyozov, L.; Uecker, A.; Serve, H.; Botzki, A.; Mahboobi, S.; Dove, S. *J. Biol. Chem.* **2003**, *278*, 5148; (d) Liu, Y.; Bishop, A.; Witucki, L.; Kraybill, B.; Shimizu, E.; Tsien, J.; Ubersax, J.; Blethrow, J.; Morgan, D. O.; Shokat, K. M. *Chem. Biol.* **1999**, *6*, 671.
31. Ostrander, J. H.; Daniel, A. R.; Lofgren, K.; Kleer, C. G.; Lange, C. A. *Cancer Res.* **2007**, *67*, 4199.
32. Linger, R. M. A.; Keating, A. K.; Earp, H. S.; Graham, D. K. *Adv. Cancer Res.* **2008**, *100*, 35.
33. (a) Sun, Y. *Mol. Carcinog.* **2006**, *45*, 409; (b) Macmillan, J. C.; Hudson, J. W.; Bull, S.; Dennis, J. W.; Swallow, C. J. *Ann. Surg. Oncol.* **2001**, *8*, 729.